Chinese Chemical Letters 37 (2026) 112207

Contents lists available at ScienceDirect

Chinese Chemical Letters

journal homepage: www.elsevier.com/locate/cclet

Poly(diphenyl carbazole)-based anion exchange membrane and ionomers for high-performance and durable anion exchange membrane water electrolysis

Qian Liu, Jinshan Han, Binghui Liu, Yang Pang, Chengji Zhao*

Key Laboratory of High Performance Plastics, Ministry of Education, College of Chemistry, Jilin University, Changchun 130012, China

ARTICLE INFO

Article history:
Received 17 May 2025
Revised 10 October 2025
Accepted 2 December 2025
Available online 3 December 2025

Keywords:
Anion exchange membrane
Poly(diphenyl carbazole)
Micro-morphology
Alkaline stability
Water electrolysis

ABSTRACT

Alkaline anion exchange membrane water electrolysis (AEMWE) is a low-cost and sustainable technology for hydrogen production. This study presents the development of high-performance anion exchange membrane (AEM) and ionomers based on quaternized poly(diphenyl carbazole) with rigid ether-bond-free aryl backbone and flexible multination strings in the side chains. The optimized molecular architecture induces pronounced microphase separation, enabling high hydroxide conductivity (159.3 mS/cm at 80 °C) and exceptional alkaline stability (1 mol/L KOH at 80 °C, retains 97.5 % ionic conductivity and 88.6 % tensile strength after 1800 h). By implementing an anode water-fed/cathode water-free configuration and regulating the structure and content of ionomers at anode and cathode electrodes, the AEMWE performance was significantly improved from 1.9 A/cm^2 to 4.2 A/cm^2 at 2 V (a 2.2-fold increase) using 1 mol/L KOH solution as the electrolyte. Under pure water conditions, the electrolyzer still achieved an excellent electrolysis performance of 1.8 A/cm^2 at 2 V. Furthermore, the fabricated AEMWE exhibited an outstanding *in-situ* durability with a low voltage degradation rate of 0.17 mV/h during a continuous operation of 1185 h at a current density of 0.5 A/cm^2.

© 2026 Published by Elsevier B.V. on behalf of Chinese Chemical Society and Institute of Materia Medica, Chinese Academy of Medical Sciences.

The growing global demand for clean energy and hydrogen economy development has driven research into efficient hydrogen production technologies [1]. Water electrolysis, particularly "green hydrogen" production using renewable energy (*e.g.*, solar, wind), offers a sustainable solution by splitting water without greenhouse emissions while mitigating renewable energy intermittency [2–5]. Traditional water electrolysis technologies mainly include alkaline water electrolyzer (AWE) and proton exchange membrane water electrolyzer (PEMWE) [6]. Although PEMWE offers high efficiency and structural compactness, its primary limitations stem from heavy reliance on precious metal catalysts including iridium (Ir) and platinum (Pt), as well as the complex manufacturing processes and high cost of perfluorosulfonic acid membranes [7,8]. Additionally, the acidic operating environment necessitates the use of corrosion-resistant titanium alloy components, further driving up overall costs [9,10]. Emerging anion exchange membrane water electrolyzers (AEMWEs) combine AWE and PEMWE advantages: compact design, non-precious metal catalysts, high current density operation, and cost efficiency [11–14]. However, this technology remains in the laboratory-based research and development stage at present due to the lack of commercially available high-performance and durable anion exchange membranes (AEMs) [15]. As the core component in an electrolyzer. The ideal AEMs should possess high hydroxide ionic conductivity, excellent resistance to degradation in strongly alkaline environments at elevated temperatures, restricted water swelling to ensure effective ion transport without compromising mechanical properties, and improved long-term durability under operating conditions [16–18].

AEMs are composed of two essential components: Polymer backbone and tethered cationic groups. The polymer backbone serves as a framework to endow AEMs with sufficient mechanical strength and thermal stability [19], whereas the cationic groups are responsible for ion transport. As research has progressed, the structural design of AEMs has been continuously optimized. The early studied AEMs containing aryl ether bonds in the backbone that are susceptible to OH^- degradation have been gradually replaced by more stable all-carbon aromatic AEMs with better tolerance in strongly alkaline environments [20,21]. Meanwhile, studies have demonstrated that the introduction of extended chains or alkyl spacers on cationic groups significantly enhances the alkaline stability of resulting AEMs [22]. Cha *et al.* [23] synthesized a quaternized polycarbazole-based AEM (QPC-TMA) with long alkyl

* Corresponding author.
E-mail address: zhaochengji@jlu.edu.cn (C. Zhao).

https://doi.org/10.1016/j.cclet.2025.112207
1001-8417/© 2026 Published by Elsevier B.V. on behalf of Chinese Chemical Society and Institute of Materia Medica, Chinese Academy of Medical Sciences.

spacer chains. After immersion in 1 mol/L KOH solution at 80 °C for 1000 h, the ion exchange capacity (IEC) and hydroxide conductivity of the QPC-TMA membrane remained unchanged. Adhikari *et al.* [24] developed a poly(diphenyl carbazole)-based AEM (PDPC-6QA), in which the spatial site resistance of alkyl chains and the high electron density effectively suppressed Hoffmann elimination of cationic groups, thus improving the alkaline stability of AEMs. However, its hydroxide conductivity is slightly lower (103 mS/cm at 80 °C) compared to those AEMs reported in literatures, and structural optimization is still needed to enhance hydroxide conductivity for achieving high current density operation in AEMWE.

To further enhance hydroxide conductivity, researchers have proposed various innovative strategies. Although increasing the IEC is a straightforward yet effective method for enhancing conductivity, the inherent contradiction between IEC and mechanical stability has led research in AEMs to focus on developing new polymer structures and optimizing material microstructures to address these challenges [25–27]. Recent studies have shown that precisely adjusting side chains can effectively balance the conductivity and stability of AEMs. Firstly, grafting cationic side chains into the polymer main chain can significantly improve ion self-assembly ability and facilitate the construction of ion channels. Li *et al.* [28] synthesized poly[(fluorene-alkylene)-*co*-(biphenyl-alkylene)] (PFBA-nC-QAs) AEMs with side chains of varying lengths. The results showed that PFBA-6C-QA achieved a hydroxide conductivity of 154 mS/cm at 80 °C. Moreover, following immersion in 2 mol/L NaOH at 80 °C for 30 days, the functional groups of PFBA-6C-QA exhibited no degradation. Additionally, by optimizing the alkyl chain length, it was found that membranes with hexyl extended chains displayed higher ion mobility rates. Additionally, the alkyl chains between cations facilitate the formation of microphase-separated structures by increasing the polarity difference between hydrophilic and hydrophobic segments, which is beneficial for enhancing hydroxide conductivity while maintaining favorable alkaline stability.

Furthermore, to enhance the electrolysis performance and durability of AEMs in practical applications, efforts should focus on the fabrication and optimization of membrane electrode assemblies (MEAs) [29]. In MEAs, the AEM and anion exchange ionomer (AEI) are recognized as critical materials influencing water electrolysis efficiency and durability, where the selection of appropriate polymer materials is essential for improving overall performance. In AEMWE systems, the oxygen evolution reaction (OER) occurs at the anode to produce oxygen and water, while the hydrogen evolution reaction (HER) takes place at the cathode to generate hydrogen and OH^- ions [30]. Many industrial AEMWE systems currently adopt an anode water-fed and cathode water-free design, which simplifies the separation of H_2O and H_2 and enhances hydrogen purity [31]. Within MEAs, the AEI primarily serves as ion transport channels between the AEM and catalysts, facilitating anion and water molecule transport. It also effectively connects catalysts, gas diffusion layers (GDLs), and the AEM, ensuring efficient ion and water transfer between components. Liquid electrolyte injected through the anode provides partial ionic conductivity to the anode, thereby reducing the requirement for AEI conductivity on the anode side. The cathode operates under relatively dry conditions, where the AEI acts as the sole ion transport pathway. Enhancing the water uptake capacity of the AEI can improve ion conduction and water diffusion, thereby optimizing electrolysis performance [32]. However, excessive water at the cathode may flood the electrode, increasing overpotential, while insufficient water may cause electrode dehydration, limit hydrogen production efficiency, and elevate local pH, accelerating material degradation [33]. Conversely, on the anode side, excessive water uptake by the AEI under continuous liquid electrolyte supply may induce significant swelling, hindering oxygen release and impairing electrolysis efficiency. Therefore, precise regulation of AEI water uptake is necessary. To advance the performance and durability of AEMWE systems, comprehensive optimization of AEM design and AEI modulation must be prioritized.

To meet the comprehensive optimization requirements for AEM design and AEI regulation, a main-chain poly(diphenyl carbazole) (PDPC) polymer without an aryl ether structure was synthesized *via* a superacid-catalyzed Friedel-Crafts alkylation reaction. Owing to the rigid molecular framework of carbazole-based materials, the resulting polymers exhibit excellent alkaline stability and effectively resist the nucleophilic attack by hydroxide ions in alkaline environments [34,35]. Concurrently, functionalized long alkyl side chains were introduced to achieve dual objectives: (1) Improving ionic conductivity by incorporating flexible alkyl spacers that induce microphase separation between hydrophobic backbones and hydrophilic quaternary ammonium groups, thereby establishing continuous ion transport channels; (2) tuning the hydrophilic-hydrophobic balance through alkyl chain functionalization, enabling precise optimization of membrane-electrode interfaces for enhanced electrolyzer performance. This molecular design establishes a structure-property relationship bridging fundamental material characteristics with practical device performance.

By varying the number of cation groups on the flexible side chains, a series of high-performance AEMs and ionomers based on quaternized poly(diphenyl carbazole) were developed (Fig. 1). Concurrently, we systematically investigated the influence of AEI structures and contents on the electrochemical performance of AEMWE, with an in-depth exploration of the water electrolysis performance and *in-situ* durability of the AEMWE. These studies provide both theoretical foundations and experimental evidence for optimizing the design and application of anion exchange membranes.

As illustrated in Fig. 1, 3,6-diphenyl carbazole and TFK were utilized to synthesize PDPC polymer *via* a superacid-catalyzed Friedel-Crafts alkylation reaction. Compared to polymers reported in other studies, PDPC exhibited a higher molecular weight, with a weight-average molecular weight (Mw) of approximately 91.9 kg/mol (Table S1 in Supporting information), enabling it to serve as a precursor material for preparing AEM with adequate mechanical strength. Subsequently, functionalized long alkyl side chains containing different numbers of quaternary ammonium (QA) groups were introduced into the polymer backbone *via* grafting reactions. These polymers were designated as PDPC-QA, PDPC-DQA, and PDPC-TQA based on the differences in their side-chain monomers.

The chemical structures of PDPC, PDPC-QA, PDPC-DQA, and PDPC-TQA were analyzed using ^{1}H NMR spectroscopy. As shown in Fig. S3a (Supporting information), the ^{1}H NMR spectrum of PDPC displays a characteristic peak corresponding to the methyl group from 1,1,1-trifluoroacetone at approximately 1.9 ppm, and a signal at 11.4 ppm assigned to the N–H group in the 3,6-diphenylcarbazole moiety. Additionally, the multiplet signals between 7.3 ppm and 8.5 ppm are attributed to the aromatic protons of the 3,6-diphenylcarbazole units. After the grafting reaction, the ^{1}H NMR spectrum of PDPC-DQA (Fig. S3b in Supporting information) reveals a new peak at 4.5 ppm, ascribed to the methylene group adjacent to the nitrogen atom in the carbazole moiety. The disappearance of the N–H group signal at 11.4 ppm confirms the complete quaternization of PDPC. The ^{1}H NMR spectra of PDPC-QA and PDPC-TQA are provided in Fig. S4 (Supporting information). The emergence of these new signals in ^{1}H NMR spectra confirmed that the quaternized polymers with varied QA cation strings were successfully synthesized.

IEC is a crucial parameter influencing the dimensional stability and the ionic conductivity of AEMs [36]. Generally, an increase in IEC enhances the ionic conductivity and water uptake of AEMs. However, excessively high IEC can lead to excessive membrane swelling, significantly compromising the dimensional stabil-

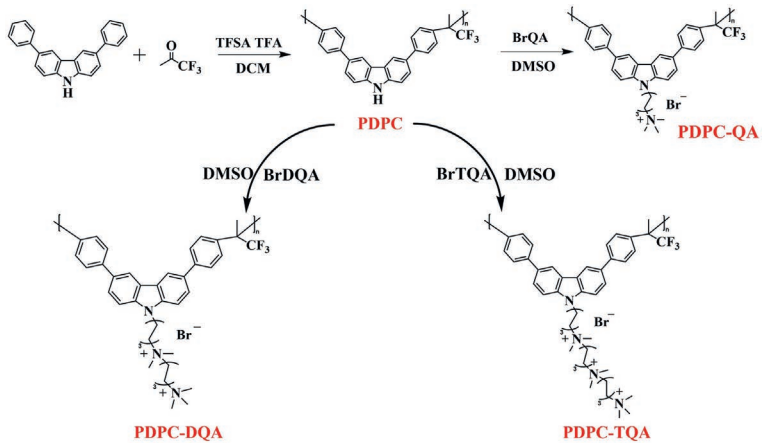


Fig. 1. Synthesis process of PDPC, PDPC-QA, PDPC-DQA, and PDPC-TQA.

ity of AEMs. Therefore, selecting an optimal IEC value is critical for balancing the ionic conductivity and dimensional stability of AEMs. As shown in Table S2 (Supporting information), the IEC values for PDPC-QA, PDPC-DQA and PDPC-TQA are 1.66, 2.68, and 3.35 mmol/g, respectively. The increase in IEC value is due to an increase in the number of cations on the side chains in the polymer. This provides more pathways for ion transport, thereby improving the conductivity of the membrane. As illustrated in Figs. S5b and c (Supporting information), the water uptake (WU) and swelling ratio (SR) of all the PDPC-QA, PDPC-DQA and PDPC-TQA membranes exhibited an increasing trend with the temperature rising. This phenomenon can be explained from the perspective of molecular motion: as the temperature rises, the thermal motion of the polymer chain segments intensifies, increasing the free volume between molecules and thereby providing more space for water uptake and membrane swelling [37]. Furthermore, the increase in temperature lowers the surface tension of water, facilitating the penetration of water molecules into the membrane matrix. At a high temperature of 80 °C, the WU values of PDPC-QA, PDPC-DQA and PDPC-TQA reached 29.5 %, 89.1 % and 273.5 %, respectively. Moreover, the hydration number (λ) values of PDPC-QA, PDPC-DQA and PDPC-TQA were 9.9, 18.5 and 45.4, respectively (Table S2), indicating a gradual increase in the number of water molecules absorbed by hydrophilic functional groups. This result is consistent with the trend of water uptake. It should be noted that due to the higher IEC value of PDPC-TQA, the membrane ruptured at 80 °C due to excessive water uptake and therefore the swelling ratio could not be characterized. Nevertheless, PDPC-TQA with high water uptake can also be used as an ionomer in the cathode of AEMWE to facilitate the transfer of water molecules from the anode to the cathode in the membrane electrode.

The stress-strain curves of three AEMs are displayed in Fig. S5d (Supporting information). It was clearly observed that the tensile strength of PDPC-QA, PDPC-DQA and PDPC-TQA membranes decreased from 64.8 MPa to 5.7 MPa, while the elongation at break increased from 9.1 % to 31.3 %. The increase in the number of cations and the length of flexible side chains weakens the entanglement interactions in the polymer main chain, thereby reducing the rigidity of the polymer and increasing the elongation at break [38]. Overall, PDPC-DQA presented a moderate mechanical strength of 21.0 MPa and a favorable elongation at break of 19.9 %. Furthermore, the thermogravimetric analysis (TGA) curves of three membranes are shown in Fig. S6 (Supporting information). It was observed that all these AEMs exhibited no thermal degradation below 200 °C. The decomposition observed between 210 °C and 380 °C was attributed to the degradation of the polymer side chains, while the thermal weight loss occurred above 380 °C was ascribed to the degradation of the polymer main chain [34]. The results revealed that the PDPC series of AEMs meets the temperature requirements for AEMWE applications.

The microphase separation behavior of AEM is synergistically influenced by side chain length and cation density. When the side chains are too short, they lack sufficient hydrophobicity and flexibility to drive hydrophilic domain aggregation, resulting in blurred microphase separation and poor ion cluster connectivity. In contrast, a moderate side chain length balances the hydrophobic-hydrophilic interaction, promotes the formation of continuous ion channels, and achieves optimal phase separation. Similarly, low cation density leads to weak inter-cation interactions, hindering the formation of continuous ion transport channels. A moderate cation density facilitates the formation of stable ion clusters, enhances the contrast between hydrophilic and hydrophobic regions, and improves both microphase separation and ionic conductivity. However, excessive cation density may cause severe ion aggregation, leading to high swelling rates and compromised dimensional stability. The microscopic morphology of PDPC-QA, PDPC-DQA and PDPC-TQA membranes was investigated using small-angle X-ray scattering (SAXS), atomic force microscopy (AFM) and transmission electron microscopy (TEM). As demonstrated in Figs. 2a-c, PDPC-QA, PDPC-DQA and PDPC-TQA membranes exhibited an obvious scattering peak in their SAXS patterns appearing at 2.1, 1.8, and 1.5 nm^{-1}, respectively. Through calculations from Bragg equation ($d = 2\pi/q$), the sizes of ionic clusters within AEMs were determined to be 2.99, 3.49, and 4.19 nm, respectively. Moreover, PDPC-DQA and PDPC-TQA membranes exhibited a more distinct scattering peak in their SAXS patterns compared to PDPC-QA, indicating the formation of well-developed interconnected hydrophilic domains induced by the incorporation of QA cation strings. As the number of cation on the flexible side chains increased, the aggregation density of hydrophilic segments increased, thereby inducing a more pronounced hydrophilic/hydrophobic phase-separated structure. However, although PDPC-TQA exhibits favorable microphase separation, the enlarged hydrophilic domains increase the swelling ratio and compromise dimensional stability. Therefore, side chain length and cation density must be synergistically optimized to balance ion transport efficiency and dimensional stability.

Figs. 2d-f show the AFM images of PDPC-QA, PDPC-DQA and PDPC-TQA, respectively. The bright areas in the images represent the hydrophobic backbone regions, while the dark areas denote the hydrophilic regions formed by QA cation strings on the flexible side chain. The indicating the presence of distinct microphase separation within the membrane. With the number of

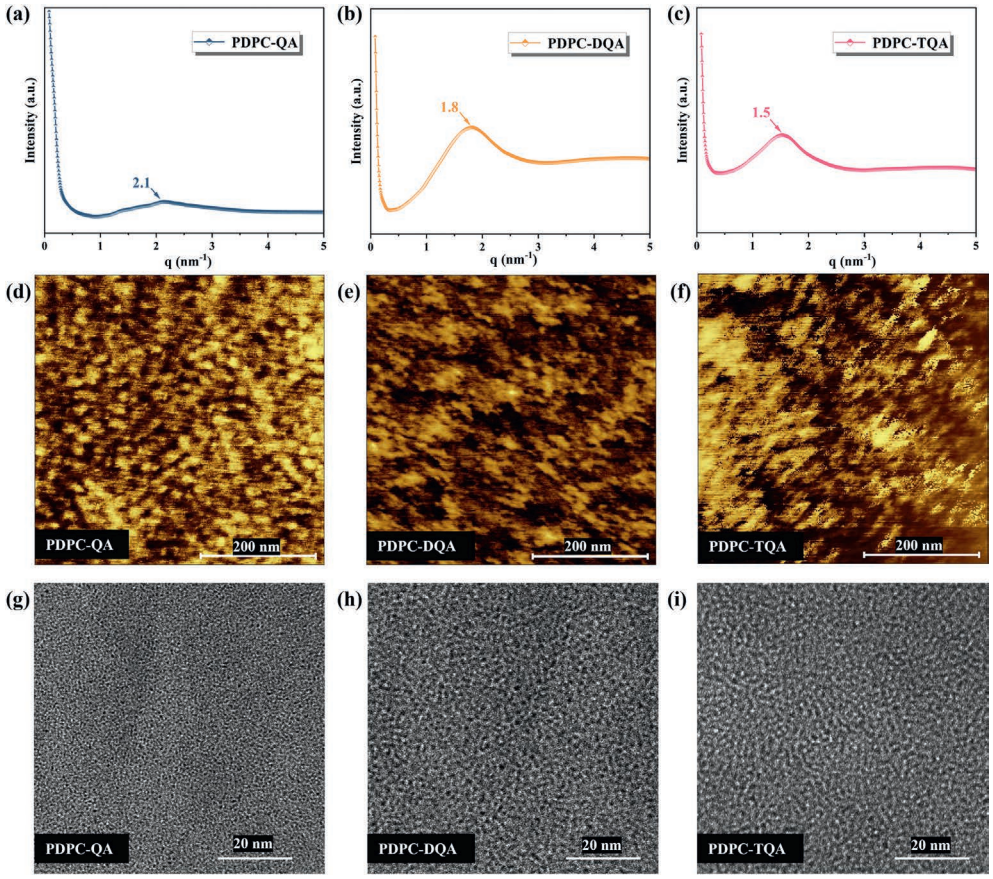


Fig. 2. SAXS patterns (a, b, c), AFM images (d, e, f) and TEM images (g, h, i) of membranes.

cation on the flexible side chains increasing, more well-defined hydrophilic/hydrophobic phase and interconnected ion transport channels were formed within these AEMs. Further morphology analysis of the AEMs was performed using TEM. As shown in Figs. 2g-i, the dark and light regions correspond to hydrophilic and hydrophobic domains, respectively, confirming the existence of distinct microphase separation within the membrane. With increased incorporation of hydrophilic functional groups, well-defined hydrophilic/hydrophobic phase boundaries and interconnected ion transport channels were observed throughout the membrane. Characterization *via* SAXS, AFM, and TEM clearly reveals that compared to PDPC-QA, the PDPC-DQA and PDPC-TQA membranes with QA cation strings demonstrated more interconnected hydrophilic domains, leading to a noticeable enlargement of hydrophilic regions. This morphology provides efficient and continuous pathways for hydroxide ion transport, thereby enhancing ion mobility and significantly improving the ionic conductivity of the PDPC-DQA and PDPC-TQA membranes.

The temperature-dependent hydroxide conductivity of PDPC-series AEMs is presented in Fig. 3a. At 30 °C, PDPC-DQA and PDPC-TQA exhibited exceptional hydroxide conductivities of 83.4 and 110.9 mS/cm, respectively, representing values approximately twice that of the PDPC-QA (43.5 mS/cm). As the temperature increases, the hydroxide conductivities of these membranes were further improved. For example, the hydroxide conductivity of PDPC-QA and PDPC-DQA increased to 87.2 mS/cm and 159.3 mS/cm at 80 °C, respectively. However, the hydroxide conductivity of PDPC-TQA at 80 °C was not measured because the membrane was excessively swollen and damaged in the test (Fig. S7 in Supporting information). As shown in Fig. 3b, when compared to other recently reported promising AEM materials, PDPC-DQA not only exhibits relatively high ionic conductivity but also maintains a low SR, indicating its ability to achieve high dimensional stability in practical applications. The superior performance of PDPC-DQA can be attributed to the presence of well-developed hydrophilic/hydrophobic phase separation as observed by SAXS, AFM and TEM. This unique morphology facilitates rapid ion transport while ensuring overall membrane stability. Considering its comprehensive performance, PDPC-DQA was chosen as the preferred membrane material to further explore its potential and effectiveness in practical AEMWE application.

The alkaline stability of AEMs is the key indicator for evaluating the durability of membrane materials in AEMWE under operational condition [48]. To comprehensively assess the alkaline resistance of the PDPC-DQA membrane, we immersed it in a 1 mol/L KOH solution and monitored the variation in the hydroxide conductivity with the immersion time at 80 °C. As shown in Fig. 3c, the hydroxide conductivity of the PDPC-DQA membrane decreased by only 2.5 % after 1800 h. Meanwhile, the membrane maintained high mechanical properties after the alkali resistance test (18.6 MPa, retaining 88.6 % of the initial tensile strength), as demonstrated in Fig. 3d. The excellent alkaline stability of the PDPC-DQA membrane can be attributed to the rigid ether-free polymer backbone and the side-chain type architecture [49]. Especially, the introduction of flexible alkyl spacers between the QA cation string and the hydrophobic polymer backbone greatly enhances the spatial site resistance to OH^- attack on the functional groups, thus improving overall alkaline resistance of the PDPC-DQA membrane [50,51]. This provides a solid foundation for the long-term stable operation in practical AEMWE employing PDPC-DQA as the AEM.

Furthermore, an accelerated alkaline stability test was employed to verify the membrane's degradation mechanism, which

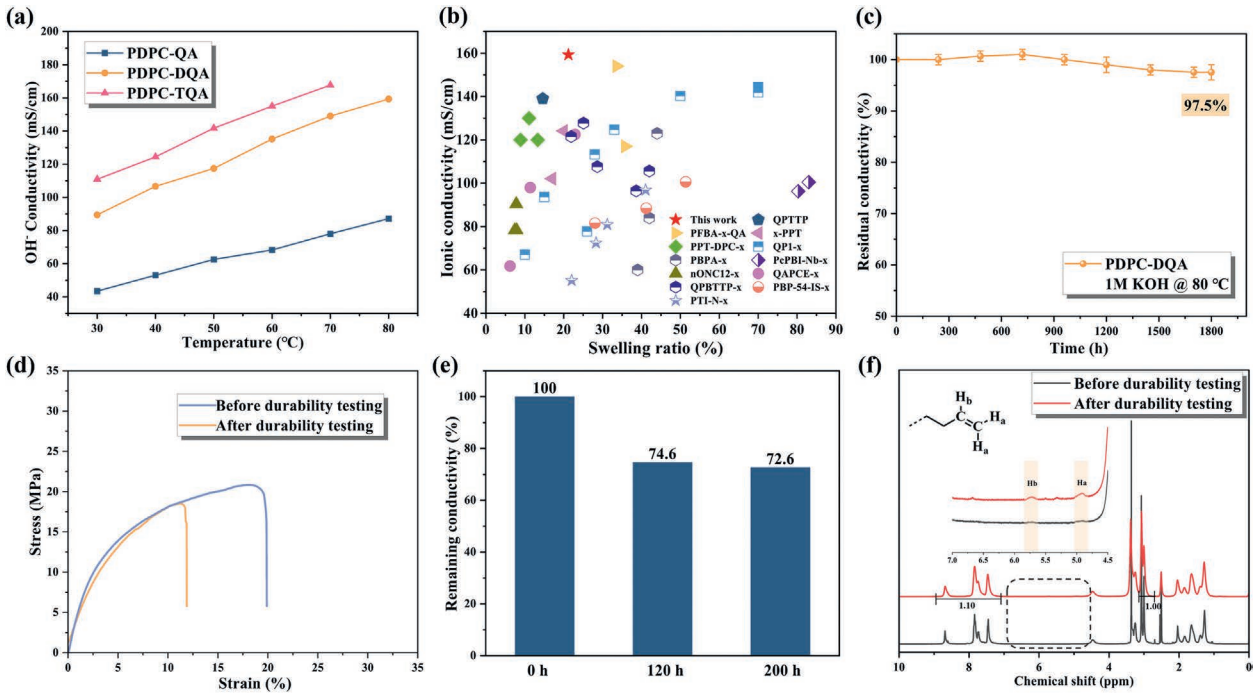


Fig. 3. The thickness of all the AEMs used is approximately 35 μm. (a) Hydroxide conductivity of PDPC-QA, PDPC-DQA and PDPC-TQA. (b) Comparison of ionic conductivity of membranes under different SR from recently published literature [20,27,28,39–47]. (c) Long-term alkali stability test of PDPC-DQA in 1 mol/L KOH at 80 °C. (d) Changes in mechanical properties of PDPC-DQA after 1 mol/L KOH alkali stability test. (e) Accelerated alkali stability test of PDPC-DQA in 5 mol/L KOH at 80 °C. (f) ^{1}H NMR spectra of PDPC-DQA after alkali stability test in 5 mol/L KOH.

was conducted in a 5 mol/L KOH solution at 80 °C. As shown in Fig. 3e, after 200 h of immersion, the membrane's hydroxide conductivity remained as high as 72.6 % of its initial value. To elucidate the potential chemical changes in the membrane under alkaline conditions, ^{1}H NMR spectroscopy was performed on the PDPC-DQA membrane before and after the accelerated alkaline resistance test (Fig. 3f). There was no evident change in the ^{1}H NMR spectrum after accelerated durability test, indicating the overall chemical structure of PDPC-DQA remained stable. However, there were two tiny signals appearing at 4.9 ppm and 5.7 ppm after magnification, which were attributed to olefins derived from the chemical degradation of QA cation string in the side chain through a typical Hofmann elimination reaction [38]. The integral area analysis revealed a 15 % degradation of quaternary ammonium groups. The exceptional alkaline stability of the PDPC-DQA membrane can be attributed to its rational molecular structure design. The rigid planar conjugated structure of 3,6-diphenylcarbazole restricts molecular rotational mobility, thereby enhancing the chemical stability of the prepared membrane [23]. Moreover, the pentyltrimethylammonium group exhibits approximately twice the stability of the piperidinium group. When incorporated into the polyaromatic main chain, the pentyltrimethylammonium moiety demonstrates high resistance to alkaline attack [52]. Furthermore, the ether-free main chain and alkyl side chain architecture effectively protects the cationic group from the effects in alkaline environments, thereby mitigating chemical degradation and ensuring long-term operational stability.

PDPC-DQA, owing to its high ionic conductivity and excellent alkaline stability, has emerged as a promising AEM for AEMWE systems. All AEMs used in this study had a thickness of approximately 35 μm. To more closely simulate industrial operating conditions, the electrolyzer was operated under an anode-fed water/cathode-dry configuration, wherein the anode is maintained in continuous direct contact with the electrolyte solution. To ensure effective gas release from the anode, anode ionomers with low water uptake and swelling rates were prioritized. This is crucial because the anode ionomer operates in high-humidity and high-temperature environments, where excessive water uptake and swelling could impede gas transport and compromise catalytic activity. Consequently, PDPC-QA and PDPC-DQA, both exhibiting low swelling ratios, were selected as candidate anode ionomer for systematic evaluation.

The anode catalyst slurry was configured with PDPC-QA and PDPC-DQA as ionomer solutions and the dispersion of the ionomer in the catalyst was observed by dynamic light scattering (DLS) test. As shown in Fig. S8 (Supporting information), the IrO_2 catalyst ink without ionomers exhibited the largest particle size with pronounced sedimentation. In contrast, the catalyst ink containing PDPC-DQA displayed a relatively larger particle size due to entanglement of its long alkyl side chains, which promoted adhesion to the catalyst surface. Notably, the PDPC-QA-containing ink demonstrated the smallest particle size (197.2 nm), indicating effective dispersion without agglomeration. Furthermore, membrane electrodes containing 25 wt% of each ionomer were fabricated for systematic evaluation in AEMWE (Fig. S9 in Supporting information). The electrolyzer employing PDPC-QA as the anode ionomer demonstrated superior performance, achieving a current density of 2.55 A/cm^2 at 2 V, which markedly exceeded that of the PDPC-DQA-based system (1.9 A/cm^2 at 2 V). This pronounced performance difference strongly suggests PDPC-QA as the optimal anode ionomer material for AEMWE applications.

In the AEMWE configuration, where the electrolyte solution flows through the anode while the cathode remains water-free, effective water transport from the anode to the cathode is critical to sustain hydrogen evolution reactions (Fig. 4a). It is required to modulate the hydrophilicity of the cathode-side electrode surface to promote the electrode reaction. Three ionomer materials were all configured as cathode catalyst slurries at 25 % and their hydrophilicity on the carbon paper electrode was observed by water contact angle test. To ensure that the cathode had enough water

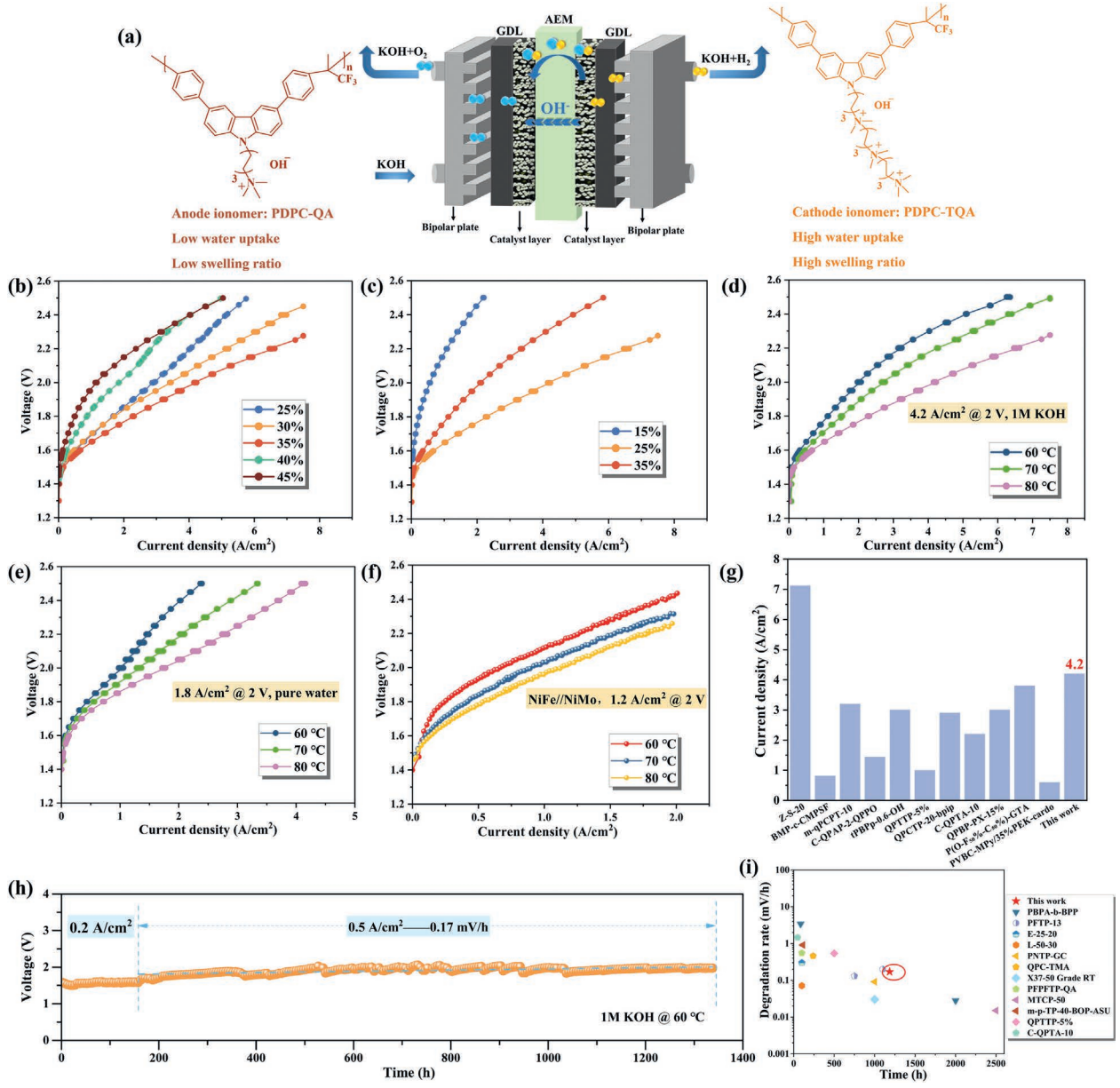


Fig. 4. (a) Schematic diagram of ionomers used and tested in AEMWE. AEMWE performance changes when varying (b) anode and (c) cathode ionomer content. AEMWE performance at different temperatures with (d) 1 mol/L KOH and (e) pure water as electrolyte. (f) AEMWE performance based on PDPC-DQA using non-precious metal catalysts. (g) Comparison of AEMWE performance with recently published literature. (h) Long-term durability test of AEMWE. (i) Comparison of voltage decay rates with reported AEMWE endurance test voltages at 500 mA/cm^2 current density conditions [13,48,53–62].

to participate in the reaction, we added 25 wt% of three different ionomers to the catalyst ink to compare the hydrophilicity of the cathode electrodes. Water contact angle measurements on carbon paper electrodes (Fig. S10 in Supporting information) showed that PDPC-DQA and PDPC-TQA had a higher water uptake capacity and smaller contact angle compared to PDPC-QA. Subsequent AEMWE performance evaluations (Fig. S9) with a 25 wt% cathode ionomer loading showed that the PDPC-TQA-based system achieved a current density of 3.0 A/cm^2 at 2 V, outperforming the PDPC-DQA counterpart (2.55 A/cm^2 at 2 V). The results demonstrated that the use of PDPC-QA as the anode ion membrane and PDPC-TQA as the cathode ion membrane could significantly improve the overall performance of AEMWE.

The PDPC-DQA-based AEMWE achieved substantial performance enhancement through parametric optimization of electrode ionomer loadings. As illustrated in Fig. 4b, the ionomer content in the fixed cathode is 25 %. The increasing content of PDPC-QA ionomer in the anode from 25 % to 45 % elevated the current density from 3.0 to 4.2 A/cm^2 at 2 V, accompanied by minimized ohmic resistance (0.04 Ω cm^2) and charge transfer resistance (0.07 Ω cm^2) (Figs. S11 and S12 in Supporting information). Upon establishing a 35 % anode ionomer loading as the optimal threshold for peak AEMWE performance, the cathodic PDPC-TQA ionomer content was systematically varied from 15 % to 35 % while maintaining the anode configuration. The PDPC-TQA ionomer exhibited optimal performance at a 25 % content (4.2 A/cm^2 at 2 V), whereas a 15 % content resulted in the lowest performance (0.57 A/cm^2 at 2 V), due to insufficient hydrophilicity that restricted reaction kinetics (Fig. 4c). Research indicates that excessive anode ionomer content can lead to a denser catalyst layer structure, obstructing the formation of gas transport channels and increasing interfacial contact impedance. When the ionomer content reaches 25 %, opti-

mal three-phase interface contact is achieved, resulting in the lowest membrane electrode resistance. Conversely, insufficient cathode ionomer content may cause cathode dehydration, while excessive content can lead to electrode flooding. Both scenarios increase the membrane electrode's impedance and reduce the performance of the electrolyzer. As shown in Figs. S13a and b (Supporting information), corresponding half-cell tests confirm the highest oxygen evolution reaction (OER) activity at a 35 % anode ionomer content and the best hydrogen evolution reaction (HER) performance at a 25 % cathode ionomer content. Additionally, as shown in Figs. S14a and b (Supporting information), lower Tafel slopes are observed when the ionomer contents of PDPC-QA and PDPC-TQA are 35 % and 25 %, respectively. A lower Tafel slope indicates that a lower overpotential is required to achieve the same current density, reflecting superior catalytic kinetics. Consequently, the optimal AEMWE configuration was determined as 35 % PDPC-QA in the anode and 25 % PDPC-TQA in the cathode.

We conducted AEMWE performance tests at varied temperatures to further evaluate the PDPC-DQA membrane. When using 1 mol/L KOH solution as the electrolyte, as shown in Fig. 4d, AEMWE achieved a high current density of 4.2 A/cm^2 at 2 V at 80 °C. Notably, even with pure water as the electrolyte, Fig. 4e shows that AEMWE still achieved a considerable current density of 1.8 A/cm^2 at 2 V. Compared to other recently reported AEMs employed in AEMWE, the prepared PDPC-DQA membrane maintains a relatively high level of electrolysis performance in both pure water (Table S4 in Supporting information) and alkaline solutions (Fig. 4g). These results demonstrate the immense potential of the PDPC-DQA membrane for AEMWE applications, performing excellently not only under strongly alkaline conditions but also maintaining efficient electrolysis performance in mild pure water environment. This characteristic provides a solid foundation for the promotion of AEMWE technology in various application scenarios, particularly showing distinct advantages in situations where the use of strongly alkaline electrolytes needs to be avoided, thereby highlighting the superiority of PDPC-DQA-based AEMWE systems.

The optimized configuration (35 % PDPC-QA anode and 25 % PDPC-TQA cathode) was further applied to a commercial AEM (FAA-3-50) and compared with the performance of electrodes incorporating commercial FAA-3 ionomer (Figs. S15a and b in Supporting information). In 1 mol/L KOH electrolyte, the MEA fabricated with the PDPC-series ionomers and FAA-3-50 membrane achieved a current density of 1.17 A/cm^2 at 2 V, substantially outperforming the MEA assembled with FAA-3 ionomer and FAA-3-50 membrane (614 mA/cm^2 @ 2 V). This result demonstrates that the ionomers developed in this work are not only compatible with the PDPC-DQA-based AEMWE system but may also exhibit broad applicability to other commercial or literature-reported AEM configurations. This experiment also included tests using non-precious metal catalysts. A nickel-iron foam nickel electrode was employed for the cathode, while a nickel-molybdenum foam nickel electrode was used for the anode. Using the catalyst-coated substrate (CCS) method, the cell achieved a performance of 1.2 A/cm^2 at 2 V and operated stably at a current density of 500 mA/cm^2 for 126 h (Fig. 4f and Fig. S16 in Supporting information).

Fig. 4h presents the long-term durability of the electrolysis cell. The durability test was conducted in two stages to comprehensively evaluate the stability and performance longevity of the PDPC-DQA-based AEMWE system under different operating conditions. The first stage was carried out under a relatively mild condition: A constant current density of 0.2 A/cm^2, a temperature of 60 °C, and a 1 mol/L KOH solution as the electrolyte. At the beginning of the test, the operating voltage of the electrolysis cell was 1.58 V. After 164 h of continuous operation, the voltage remained almost unchanged, demonstrating the system's excellent stability under this mild condition. In the second stage, the constant current density was significantly raised from 0.2 A/cm^2 to 0.5 A/cm^2, resulting in a corresponding increase in the operating voltage of the electrolysis cell. The durability test continued for an extended period of 1185 h, the voltage decay rate was calculated to be 0.17 mV/h, which was comparable and even lower than those reported recently (Fig. 4i). These results demonstrate the PDPC-DQA-based AEMWE system possesses outstanding stability with an acceptable decay rate under long-term, high-intensity operating conditions.

Poly(diphenyl carbazole) with a rigid ether-free main chain was successfully synthesized through superacid-catalyzed polycondensation, and a series of anion exchange membrane and ionomers based on quaternized poly(biphenyl carbazole) were prepared by introducing long alkyl side chains with cation strings. This meticulously designed molecular structure aimed to optimize the performance of AEMWE systems. Systematic evaluation results indicated that ionomer content significantly influenced AEMWE performance. Additionally, the developed PDPC-DQA exhibited a distinct microphase separation structure, effectively reducing OH^- ion transport resistance and achieving an ionic conductivity as high as 159.3 mS/cm at 80 °C. Meanwhile, it demonstrated exceptional alkaline stability, retaining 97.5 % of its initial ionic conductivity and 88.6 % of its tensile strength after 1800 h of immersion in 1 mol/L KOH solution at 80 °C. For water electrolysis applications, the PDPC-DQA-based AEMWE achieved a high current density of 4.2 A/cm^2 at 2 V with a 1 mol/L KOH solution as the electrolyte. Notably, even with pure water as the electrolyte, the AEMWE still attained a considerable current density of 1.8 A/cm^2 at 2 V. During durability tests, at a current density of 0.2 A/cm^2 and 0.5 A/cm^2, the system operated continuously for 1349 h with a voltage degradation rate of only 0.17 mV/h, demonstrating excellent in-situ durability. In summary, the developed quaternized poly(diphenyl carbazole) based AEM and ionomers exhibit outstanding performance in mechanical strength, ionic conductivity, alkaline resistance, as well as electrolysis performance and long-term durability. This research provides new material options for the further development and practical application of AEMWE technology.

Declaration of competing interest

The authors declare that they have no known competing financial interests or personal relationships that could have appeared to influence the work reported in this paper.

CRediT authorship contribution statement

Qian Liu: Writing – original draft, Methodology, Investigation, Data curation. **Jinshan Han:** Investigation. **Binghui Liu:** Investigation. **Yang Pang:** Validation. **Chengji Zhao:** Writing – review & editing, Supervision, Funding acquisition, Conceptualization.

Acknowledgments

This research was financial supported by the National Natural Science Foundation of China (No. 22579067 and No U24A20505). The authors sincerely thank Paul A. Kohl from the Georgia Institute of Technology for his generous support and advice during the project.

Supplementary materials

Supplementary material associated with this article can be found, in the online version, at doi:10.1016/j.cclet.2025.112207.

References

[1] F. Ueckerdt, P.C. Verpoort, R. Anantharaman, et al., Joule 8 (2024) 104–128.
[2] H. Liu, L.R. Clausen, L. Wang, M. Chen, Energy Environ. Sci. 16 (2023) 2090–2111.
[3] H. Lin, Q. Wu, X. Chen, et al., Renew. Energy 173 (2021) 569–580.
[4] N.A. Burton, R.V. Padilla, A. Rose, H. Habibullah, Renew. Sustain. Energy Rev. 135 (2021) 110255.
[5] R.T. Liu, Z.L. Xu, F.M. Li, et al., Chem. Soc. Rev. 52 (2023) 5652–5683.
[6] N. Hassan, A. Jalil, S. Rajendran, et al., Int. J. Hydrogen Energy 52 (2024) 420–441.
[7] I. Arunkumar, M.M. Rana, A. Jeevitha, et al., ACS Sustain. Chem. Eng. 12 (2024) 9361–9375.
[8] R. Gokulapriyan, S. Karthikeyan, D.J. Yoo, J. Mater. Chem. A 12 (2024) 23880–23896.
[9] I. Arunkumar, R. Gokulapriyan, V. Sakthivel, et al., ACS Appl. Energy Mater. 6 (2023) 7702–7713.
[10] R. Gokulapriyan, B.H. Kim, S. Vijayapradeep, et al., J. Membr. Sci. 700 (2024) 122692.
[11] M.J. Jang, S.H. Yang, M.G. Park, et al., ACS Energy Lett. 7 (2022) 2576–2583.
[12] N. Du, C. Roy, R. Peach, et al., Chem. Rev. 122 (2022) 11830–11895.
[13] N. Chen, S.Y. Paek, J.Y. Lee, et al., Energy Environ. Sci. 14 (2021) 6338–6348.
[14] Y. Zheng, A. Serban, H. Zhang, et al., ACS Energy Lett. 8 (2023) 5018–5024.
[15] C. Liu, Z. Geng, X. Wang, et al., J. Energy Chem. 90 (2024) 348–369.
[16] G.W. Ryoo, S.H. Park, K.C. Kwon, et al., J. Energy Chem. 93 (2024) 478–510.
[17] L. Wan, J. Liu, D. Lin, et al., Energy Environ. Sci. 17 (2024) 3396–3408.
[18] Y. Ma, L. Li, X. You, et al., Chem. Eng. J. 480 (2024) 148225.
[19] K.M. Hugar, W. You, G.W. Coates, ACS Energy Lett. 4 (2019) 1681–1686.
[20] Z. Jiang, G. Yi, X. Yao, et al., Chem. Eng. J. 467 (2023) 143442.
[21] W.T. Gao, X.L. Gao, Y.S.L. Choo, et al., Chem. Eng. J. 466 (2023) 143107.
[22] L. Liu, W. Ma, J. Zhang, et al., J. Membr. Sci. 678 (2023) 121663.
[23] M.S. Cha, J.E. Park, S. Kim, et al., Energy Environ. Sci. 13 (2020) 3633–3645.
[24] S. Adhikari, I. Matanovic, D. Leonard, et al., ACS Macro Lett. 13 (2024) 28–33.
[25] Y. Lee, K. Min, J. Choi, et al., J. Mater. Chem. A 11 (2023) 25008–25019.
[26] C. Hu, N.Y. Kang, H.W. Kang, et al., Angew. Chem. Int. Ed. 63 (2024) e202316697.
[27] Y. Zhang, F. Zhang, Y. Chen, et al., Chem. Eng. J. 455 (2023) 140938.
[28] X. Li, K. Yang, Z. Li, et al., Int. J. Hydrogen Energy 47 (2022) 15044–15055.
[29] L. Wan, Z. Xu, Q. Xu, et al., Energy Environ. Sci. 16 (2023) 1384–1430.
[30] S. Oh, H. Roh, H. Im, et al., Chem. Eng. J. 500 (2024) 157106.
[31] K. Ham, S. Bae, J. Lee, J. Energy Chem. 95 (2024) 554–576.
[32] Y. Yang, P. Li, X. Zheng, et al., Chem. Soc. Rev. 51 (2022) 9620–9693.
[33] J.E. Park, S.Y. Kang, S.H. Oh, et al., Electrochim. Acta 295 (2019) 99–106.
[34] Q. Li, L. Wu, Y. Pang, et al., Macromol. Rapid Commun. 45 (2024) 2300734.
[35] Y. Pang, Q. Li, B. Liu, et al., Chem. Eng. J. 499 (2024) 156473.
[36] G. Deng, Y. Liao, Y. Lin, et al., Angew. Chem. Int. Ed. 63 (2024) e202412632.
[37] Y. Zheng, U. Ash, R.P. Pandey, et al., Macromolecules 51 (2018) 3264–3278.
[38] F. Liu, K. Miyatake, M. Tanabe, et al., Adv. Sci. 11 (2024) 2402969.
[39] S.Q. Fu, B. Hu, J.H. Ge, et al., Macromolecules 56 (2023) 6037–6050.
[40] J.H. Chen, Y.S.L. Choo, X.H. Wang, et al., J. Colloid Interface Sci. 638 (2023) 62–72.
[41] Y.J. Liu, W.T. Gao, A.M. Zhu, et al., J. Membr. Sci. 687 (2023) 122045.
[42] M. Guo, T. Ban, Y. Wang, et al., J. Colloid Interface Sci. 638 (2023) 349–362.
[43] C. Wei, W. Yu, Y. Zhang, et al., J. power sources 553 (2023) 232247.
[44] Y. Niu, J. Li, W. Yu, et al., Mater. Today Commun. 38 (2024) 108241.
[45] J. Wu, J. Zhao, N. Li, et al., Int. J. Hydrogen Energy 62 (2024) 1043–1053.
[46] Y. Gu, Y. Zhang, Z. Wang, et al., Ind. Chem. Mater. 2 (2024) 141–153.
[47] Y. Gu, T. Dong, Y. Zhang, et al., J. Power Sources 592 (2024) 233918.
[48] W. Song, K. Peng, W. Xu, et al., Nat. Commun. 14 (2023) 2732.
[49] A.S. Hameed, S. Munusamy, R. Gokulapriyan, et al., ACS Appl. Polym. Mater. 6 (2024) 12341–12361.
[50] H.S. Dang, P. Jannasch, J. Mater. Chem. A 4 (2016) 17138–17153.
[51] H.S. Dang, P. Jannasch, Macromolecules 48 (2015) 5742–5751.
[52] Q. Ling, C. Wang, T. Wang, et al., ChemSusChem 17 (2024) e202301656.
[53] A.L.G. Biancolli, B. Chen, A.S. Menandro, et al., J. Mater. Chem. A 12 (2024) 21442–21454.
[54] J. Zhang, J. Pan, Y. Yuan, et al., Chem. Mater. 36 (2024) 5720–5729.
[55] J. Hyun, S.H. Yang, D.W. Lee, et al., Chem. Eng. J. 469 (2023) 143919.
[56] S. Han, J. Park, J. Yoon, Adv. Funct. Mater. 34 (2024) 2314573.
[57] H. Lim, G.H. Han, D.H. Lee, et al., Small 20 (2024) 2400031.
[58] S. Zhang, W. Ma, L. Tian, et al., ACS Appl. Mater. Interfaces 16 (2024) 7660–7669.
[59] S. Zhang, X. Li, Y. Yang, et al., J. Membr. Sci. 698 (2024) 122587.
[60] X. Wang, F. Chen, Y. Gao, et al., J. Membr. Sci. 718 (2025) 123693.
[61] Y. Ma, C. Hu, G. Yi, et al., Angew. Chem. Int. Ed. 62 (2023) e202311509.
[62] D. Li, A.R. Motz, C. Bae, et al., Energy Environ. Sci. 14 (2021) 3393–3419.